Dynamic Estimation of Load-Side Equivalent Inertia by Using Clustering Method

Yunlu LI, Shuang GUO, Guiqing MA, Zhenyu LI, Junyou YANG, and Zhe CHEN

***Abstract*—With the increasing share of renewable energy and power electronics, the power system is gradually showing the characteristics of low inertia and spatial distribution. This transition deteriorates system's frequency response and poses a major threat to system stability. The majority of research in this area investigates the methods of providing inertia from the supply side. However, the load response also plays a crucial role in determining the frequency response. Hence, in depth knowledge about the amount of inertia provided by load is extremely important for a future application of units supplying synthetic inertia. In order to accurately grasp the load inertia level, a data-driven equivalent inertia aggregation estimation method is proposed. To achieve the load-side inertia aggregation estimation under different fault scenarios, a dynamic aggregating method is proposed, which uses the *K*-means algorithm to aggregation the grid based on load-side spectral features. Then, according to voltage dependency and rotating characteristic under disturbances, an area inertia estimation model is constructed to estimate the inertia of the aggregated area. By applying the proposed method, the accuracy of inertia estimation under multiple operating conditions is increased by considering the dynamic behaviour of inertia distribution. Finally, using the IEEE 29 buses system, the proposed method is illustrated.**

***Index Terms*—Data-driven, equivalent inertia, inertia estimation, load-side inertia, system aggregation.**

I. Introduction

RENEWABLE energy sources (RES) continue to penetrate the power system. Due to the absence of rotating equipment or power electronic devices and grid frequency decoupling, the inertia of the power system decreases, leading to insufficient inertia support. This situation causes power system instability and decreases anti-interference ability [1]–[4]. Upon a disturbance, the primary frequency modulation (FM) response is delayed. Inertia initially plays a crucial role in maintaining system stability [5]. Additionally, instances where the system's inertia support is insufficient to resist fault disturbances occur periodically. Therefore, accurately calculating the power system's inertia level is key to overall stable operation, control, and scheduling. Its magnitude is strongly correlated with the rate of change of frequency (ROCOF) [6]–[7]. ROCOF decreases as the power system's inertia increases, benefiting system stability. Consequently, it serves as a metric for estimating inertia. However, most existing studies primarily focus on estimating inertia provided by the generation side, with limited attention given to estimating load-side inertia.

In depth knowledge of inertia provided by the power load side is crucial for the future application of units supplying synthetic inertia. It promotes technical efficiency and cost effective application. In [8], the average inertia constant of the demand side for the UK power system accounts for 20% of the total inertia, highlighting the significant contribution of demand-side inertia. Understanding load-side inertia can benefit system operators in managing load shedding. Inertia impacts ROCOF and system stability. To prevent system frequency instability, load fluctuations are mitigated by load shedding. Prioritizing high-inertia loads and avoiding their shedding during contingencies could improve system reliability.

Several recent studies have addressed load side inertia estimation. In [9], a white-box method is proposed for calculating the load inertia of the Irish power system. The load inertia is extracted from the system overall inertia by subtracting the contribution from the generators. In [8], historical data of grid frequency outage events are used to estimate the inertia contribution of the demand side. In [10], an online estimation method is proposed to monitor the time-varying inertia of the loads, under normal operating conditions. These methods treat the load side as a whole, do not further investigate inertia in different regions of the load side. In [11], the load inertia contribution from different power consumers is studied in detail following a blackout in the city of Flensburg. However, this approach estimates inertia by considering the categories of power consumers without accounting for the geographic distribution of power consumers. In [12], under HVDC power disturbances, the inertia contribution from power station auxiliary loads is considered in the overall system inertia. However, this study reflects the system inertia without estimating the contribution of load side individually. In summary, while recent studies explore load side inertia, a clear distinction from generation side inertia is needed. The unique technical challenges of load side inertia evaluation, such as accounting for variability across

Manuscript received March 8, 2024; revised June 12, 2024 and November 12, 2024; accepted January 3, 2025. Date of publication March 30, 2025; date of current version January 20, 2025. This work was supported by the 111 Project under the grant D23005. *(Corresponding author: Yunlu Li.)*

Y. Li, S. Guo, G. Ma, Z. Li, and J. Yang are with the School of Electrical Engineering, Shenyang University of Technology, Liaoning 110819, China (e-mail: liyunlu@sut.edu.cn; Shuangguo@smail.sut.edu.cn; guiqingma@smail.sut.edu.cn; 2693570568@smail.sut.edu.cn; junyouyang@sut.edu.cn).

Z. Chen is with the Department of Energy Technology, Aalborg University, 9220, Denmark (e-mail: zch@et.aau.dk).

Digital Object Identifier 10.24295/CPSSTPEA.2025.00001

various types and geographic distribution, require specialized methods that diverge from traditional generator-focused approaches. The inertia of large systems is characterized by a complex spatial distribution. Estimating inertia levels in different regions can provide a more refined reference for system operation and control. Inertia estimation that does not consider spatial distribution characteristics may result in poor system robustness and low accuracy of the estimation results.

Recently, several studies estimate the regional inertia by considering the spatial distribution characteristics of inertia. In [13], the power change of the loads due to voltage dependency is estimated after a disturbance. By utilizing total generated power and voltage data from the generator buses, the area inertia is calculated separately. In [14], the effective inertia of power system area is estimated based on energy variations. In [15], a data-driven equivalent inertia partition estimation method is proposed to accurately capture the system inertia level. These studies considered the regional distribution of inertia, but their system partitioning focused on the generation side and remained fixed. The spatial distribution characteristics of inertia play an important role in inertia assessment. In [16], based on the center of inertia (COI) concept, a practical study on inertia distribution estimation is presented using oscillation index and center of frequency index. In [17], the in-homogeneity of the propagation speed of electromagnetic waves is used to propose a method for detecting changes in the inertia distribution of a power system. In [18], the relationship between inertia distribution, system oscillation and power electronic interface position is investigated, the concept of inertia distribution index (IDI) is proposed to reveal the relationship between inertia and centre of inertia in each region under large disturbances. However, few studies have estimated the load side regional inertia by considering spatial distribution characteristics. Considering the spatial distribution characteristics of inertia in load inertia estimation is the key issue addressed in this paper.

This article aims to estimate the equivalent inertia of each area of load side system based on data-driven technology. The main contributions of this article are as follows.

1) A data-driven inertia estimation framework for load side power system was established, which dynamically clustering according to different spatial distribution characteristics during various transient behaviors.
2) Considering the power variations affected by voltage disturbance, influence among inertia, power and frequency is revealed.
3) The advantages of the proposed method are demonstrated by IEEE 29 buses system on MATLAB/Simulink platform.

The remainder of the paper is structured as follows. Section II details the load side clustering model, analyzes the inertia spatial distribution characteristics and the load-side inertia components, describes the equivalent inertia estimation model used in this paper. Section III illustrates the study cases and simulation results, Section IV concludes the paper.

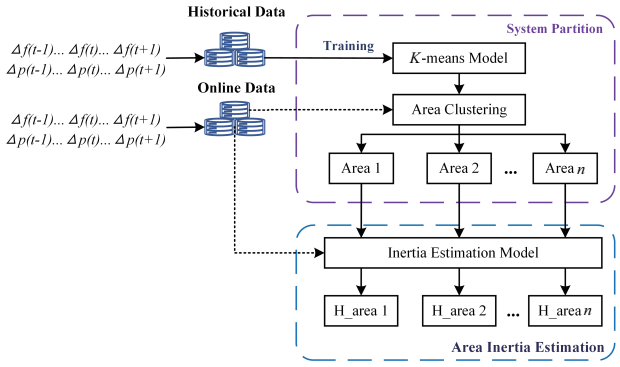

Fig. 1. The framework of inertia estimation.

II. Data-Driven Equivalent Inertia Estimation of Load-Side System

Fig. 1 illustrates the structured approach for estimating area-specific inertia. The process consists of three main steps, each with specific inputs, processes, and outputs. First, historical data containing frequency response information serves as the input to the *K*-means model, where spectral features are extracted to form distinct inertia regions. This trained model is then applied to online data for real-time area clustering, assigning data points to equivalent inertia areas. Finally, these clustered areas are fed into the inertia estimation model, which utilizes real-time data to calculate the equivalent inertia for each region. This structured framework ensures a comprehensive approach to estimating area-specific inertia dynamically and accurately.

A. The Spatial Distribution of Inertia Characteristic

The low inertia characteristics of the high ratio converter access region are significant and contrast with the high inertia posture of the synchronous power clusters distribution region. The system inertia exhibits distinct spatial distribution characteristics, making the assessment of inertia adequacy and its distribution crucial. Therefore, it is necessary to consider the regional distribution of inertia in such assessments.

In this paper, based on the definition of inertia distribution index (IDI) [16]–[19], it is discrete and used to illustrate the spatial distribution of system inertia. The electrical distance d_{k} is calculated as follows:

$$d_{\mathrm{k}} = \sum_{i=1}^{M} \Delta T \cdot [f_{\mathrm{k}}(i) - f_{\mathrm{COI}}(i)]^2 \tag{1}$$

where d_{k} is the electrical distance between node k and the centre of inertia, M is the number of samples, ΔT is the sampling interval of phase measurement unit. $f_{\mathrm{k}}(i)$, $f_{\mathrm{COI}}(i)$ are the node k frequency value and the centre of inertia frequency value. $M \cdot \Delta T$ is the calculation lengths corresponding to the IDI index, referring to the time interval between the occurrence of the disturbance and the time before frequency modulation of the unit.

The deviation of the node frequency from the centre of iner-

tia frequency is compared after a disturbance occurs. The node with the smallest deviation in frequency is defined as the centre of inertia. The centre of inertia frequency $f_{\mathrm{COI}}(t)$ is calculated as follows:

$$f_{\mathrm{COI}}(t)=\frac{\sum_{i\in n}H_{\mathrm{G}i}\cdot f_{\mathrm{G}i}(t)}{\sum_{i\in n}H_{\mathrm{G}i}} \tag{2}$$

where $f_{\mathrm{G}i}(t)$ is the frequency of generator node *i*.

The next step is to normalize the electrical distance d_{k} to obtain the node inertia distribution index.

$$I_{\mathrm{Dlk}}=\frac{d_{\mathrm{k}}-d_{\max}}{d_{\max}-d_{\min}} \tag{3}$$

where I_{Dlk} is the value of the inertia distribution index corresponding to node *k*. $d_{\max}$, $d_{\min}$ are the maximum and minimum electrical distance between the node and the centre of inertia.

After a disturbance occurs, the center of inertia frequency deviation exhibits less deviation compared to the frequency deviations of other nodes. Therefore, the center of inertia frequency can be used as a benchmark. The magnitude of node inertia is determined by comparing the frequency deviation between the node and the center of inertia. The smaller the value of I_{Dlk}, the closer node *k* is to the center of inertia, indicating a higher node inertia .

In general, the frequency response of the power system exhibits spatial distribution characteristics. The distribution of inertia across different areas significantly impacts these frequency response characteristics. Inspired by this, and to meet the requirement for accurate assessment of low-inertia systems, this paper dynamically clusters the system based on frequency response characteristics and comprehensively quantifies the system's inertia characteristics.

B. Load-Side Clustering

As renewable generation increases in interconnected power systems, the distribution of inertia becomes uneven, impacting load frequency response. To address this issue, a data-driven clustering method is proposed, based on time-series operational data of the power system. This method establishes a mapping between real-time measurement data and equivalent inertia, enabling dynamic estimation of inertia across the system.

To enhance the model's sensitivity to load behavior, load electrical parameters, resistance (*R*), inductance (*L*), and capacitance (*C*) are incorporated, alongside frequency response data. For each load, historical frequency data L is transformed into the frequency domain. By applying the fast fourier transform (FFT), the frequency spectrum $F(\omega)$ is derived:

$$F(\omega)=\frac{1}{T}\left|\int_0^T X(t)e^{-\mathrm{j}\omega t}\mathrm{d}t\right| \tag{4}$$

where T=40000 represents the sample count. Key features, including the peak value V and corresponding frequency ω_{peak} are extracted from $F(\omega)$:

$$V=\max\left(F(\omega)\right),\omega_{\mathrm{peak}}=\arg\max F(\omega) \tag{5}$$

Additionally, the standard deviation σ of $F(\omega)$ is calculated to quantify the frequency spread:

$$\sigma=\sqrt{\frac{1}{T}\sum_{\omega}(F(\omega)-\mu)^2},\mu=\frac{1}{T}\sum_{\omega}F(\omega) \tag{6}$$

The extracted features V, ω_{peak}, and σ are compiled into a feature matrix $\boldsymbol{N}$, which is subsequently clustered using the *K*-means algorithm with M=4 clusters, representing different inertia categories.The detailed procedure is shown in Tables I and II. The effectiveness of this clustering approach is demonstrated using the IEEE 29-bus system, providing insights into inertia distribution and its influence on frequency stability.

TABLE I
CLUSTERING ALGORITHM

Algorithm: Data-driven clustering
Input: **L** (400000*13)
Output: **idx**
1: **X(t)**←**L**
2: **for** *i*=1,...,13
3: F = $\left|\int X(t)e^{-\mathrm{j}\omega t}\mathrm{d}t\right|$ / 40000
4: **end for**
5: [**V**, **I**]=max(**F**)
6: **N**(*i*,1)=**V**
N(*i*,2)=**I**
N(*i*,1)=std(**F**)
7: **M**=4
8: **idx**←K-means(**N**,**M**)

TABLE II
LOAD RLC PARAMETERS

Load	*R*	*L*	*C*
Load 1	41×10^5	330×10^6	0
Load 2	43×10^5	990×10^6	0
Load 3	45×10^5	1650×10^6	0
Load 4	33×10^5	990×10^6	0
Load 5	44×10^5	1320×10^6	0
Load 6	44×10^5	1320×10^6	0
Load 7	22×10^5	660×10^6	0
Load 8	66×10^5	1980×10^6	0
Load 9	11×10^5	330×10^6	0
Load 10	22×10^5	660×10^6	0
Load 11	22×10^5	660×10^6	0
Load 12	3×10^9	0	5.2×10^6
Load 13	8×10^9	0	5000×10^6

C. Equivalent Inertia Analysis and Estimation

Load-side inertia evaluation presents distinct challenges compared to generation-side inertia. Unlike the relatively uni-

form inertia of synchronous generators, load-side inertia varies due to the diverse nature of loads, such as synchronous motors, asynchronous motors, and static loads, each responding differently to frequency disturbances. This variability, along with the need to capture dynamic behavior across regions and varying conditions, complicates accurate measurement and modeling of load-side inertia. The energy stored in the electromagnetic fields and rotating components of load equipment responds instantly to frequency deviations, stabilizing the system and providing crucial time for primary frequency modulation (FM) [20]−[25]. These complexities necessitate advanced data-driven and dynamic modeling approaches to effectively assess load-side inertia.

Motor load is primarily characterized by its rotational power, providing rotational inertia to the system. This characteristic implies that when there is a power imbalance in the system, the rotor shaft of the equipment decelerates, converting the mechanical energy stored in the rotor into electrical energy, thereby affecting the system's power balance. Since most loads are asynchronous motors with complex mechanical and electromagnetic characteristics, the overall inertia on the load side is inherently time-varying.

Static load, on the other hand, is characterized by its voltage-power relationship, providing voltage characteristic inertia to the system. The power changes in response to voltage fluctuations, compensating for power imbalances and mitigating frequency changes in the system.

As mentioned above, it is concluded that the inertia effects from different sources collectively influence the power changes in the load. Therefore, the equivalent inertia of a load is quantified by the rate of change in its power.

Power system rotational inertia refers to the energy stored in the rotating shaft of a machine at rated speed. The inertia constant H for a single mechanical shaft is calculated as follows:

$$H = \frac{J\omega_{\mathrm{n}}^2}{2S_{\mathrm{B}}} \tag{7}$$

where H is in s, J is the moment of inertia in kg·m^{2}s, S_{B} is the rated capacity and ω_{n} is the rated speed.

When there is a power imbalance in the system, frequency changes occur. The rotational kinetic energy of the rotor responds by decreasing the rotor speed and, consequently, the frequency. The rate of frequency change depends on variations in active power and system inertia. The dynamic behavior of system frequency is described by the equation of motion for the rotating mass.

$$2H\frac{\mathrm{d}f(t)}{\mathrm{d}t} = P_{\mathrm{m}}(t) - P_{\mathrm{e}}(t) = \Delta P_{\mathrm{a}} \tag{8}$$

where P_{m} is the mechanical power to drive the shaft of rotor in p.u., P_{e} is the power through machine air gap in p.u.. Thus, the single device rotating inertia is obtained.

$$H = \frac{\Delta P_{\mathrm{a}}(t)}{2\dfrac{\mathrm{d}f(t)}{\mathrm{d}t}} \tag{9}$$

As in (9), it defines the relationship between power and frequency for the rotating inertia, but it accounts for the sum power of the rotating mass. However, since the load side comprises not only asynchronous motors but also static loads, which have voltage-power characteristics, ΔP_{a} alone cannot represent the power change in static loads due to voltage fluctuations. Another quantity is needed to represent the power change in static loads.

$$\Delta P_{\mathrm{L}} = P_{\mathrm{L0}}[k_z(\frac{U_{\mathrm{L}}}{U_{\mathrm{L0}}})^2 + k_i(\frac{U_{\mathrm{L}}}{U_{\mathrm{L0}}}) + k_p] \tag{10}$$

where P_{L0} is the load active power before disturbance, U_{L} is the load node voltage, k_z is the constant impedance load ratio, k_i is the constant current load ratio, k_p is the constant power load ratio.

In summary, the load inertia of a region comprises both rotational inertia and voltage characteristic inertia. The total power change in an area equals the sum of the power changes of each device within it. After a disturbance, the frequency does not have a unique value across the entire area, necessitating the definition of a representative average frequency signal for the system. This signal is represented by f_{coi}.

$$f_{\mathrm{coi}}(t) = \frac{\sum f(t)}{n} \tag{11}$$

where $f(t)$ is the frequency variation of each device in the area, n is the number of devices in the area. Therefore, the area equivalent inertia is defined as follows:

$$H_{\mathrm{area}} = \frac{\sum \Delta P_{\mathrm{a}}(t) + \Delta P_{\mathrm{L}}}{2\dfrac{\mathrm{d}f_{\mathrm{coi}}(t)}{\mathrm{d}t}} = \frac{\sum \Delta P}{2\dfrac{\mathrm{d}f_{\mathrm{coi}}(t)}{\mathrm{d}t}} \tag{12}$$

According to (12), the error of H_{area} is directly related to the error of f_{coi} in the area. The f_{coi} represents the average response level of all load inertia in the area. The traditional method artificially divides an area with different load inertia response levels, making $f_{\mathrm{coi\_tra}}$ values difficult to accurately represent the true value levels of all loads in the area, leading to an error $\Delta f_{\mathrm{coi\_tra}}$. The proposed clustering method divides the loads with similar frequency responses into an area, where the $f_{\mathrm{coi\_pro}}$ values are closer to the true values, resulting in a smaller error $\Delta f_{\mathrm{coi\_pro}}$. Consequently, $\Delta f_{\mathrm{coi\_tra}} > \Delta f_{\mathrm{coi\_pro}}$.

To achieve this aim, simulation validation is conducted to compare the error and cumulative error of the two methods. Additionally, mean absolute error (MAE) and root mean square error (RMSE) are introduced to quantify the improved accuracy of the proposed method. The detailed data demonstrate that the accuracy of the proposed method is improved across several dimensions.

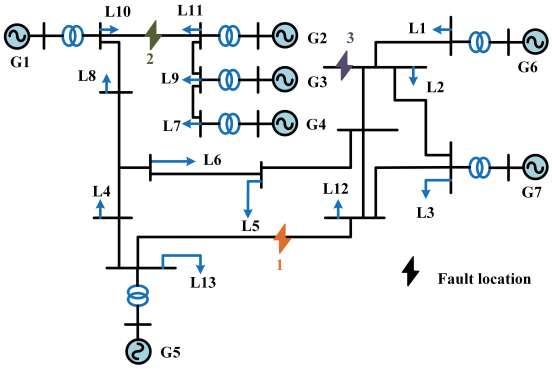

Fig. 2. System architecture diagram.

TABLE III
GENERATOR PARAMETERS

Generator	*S*/MVA	*P*/MW	Inertia/s	Type
G1	5500	—	6.4	swing
G2	2200	1800	7	PV
G3	200	180	7	PV
G4	2700	2500	8	PV
G5	5000	4500	6	PV
G6	5900	5000	7	PV
G7	4900	4500	7	PV

TABLE IV
LOAD PARAMETERS

Load	*P*/MW	*Q*/Mvar
L1	1.1	330
L2	3.3	990
L3	5.5	1650
L4	3.3	990
L5	4.4	1320
L6	4.4	1320
L7	2.2	660
L8	6.6	1980
L9	1.1	330
L10	2.2	660
L11	2.2	660
L12	6009	5.2
L13	15500	3001.2

III. CASE STUDY

A. Configuration Setup

The system depicted in Fig. 2 is constructed using the MATLAB/Simulink platform. The simulation hardware used is a PC equipped with an Intel® Core (TM) i7-1250 CPU and 16 GB of RAM. The nominal frequency is set to 50 Hz, the simulation sampling points is 7.5×10^{-5} s. Detailed parameters of the system are presented in Tables III and IV.

B. Load-Side Area Equivalent Inertia Estimation

Following the method outlined in Section II, frequency data from 13 loads are sampled within 0 to 1.2 s of the system frequency fault occurrence. These frequency response samples are then constructed, trained, and clustered, with the number of categories selected as K=4. Additionally, three-phase short-circuit faults are set to occur in three different locations. The clustering results of the frequency response curves are depicted in Fig. 3, while the load side clustering results are presented in Figs. 4–6.

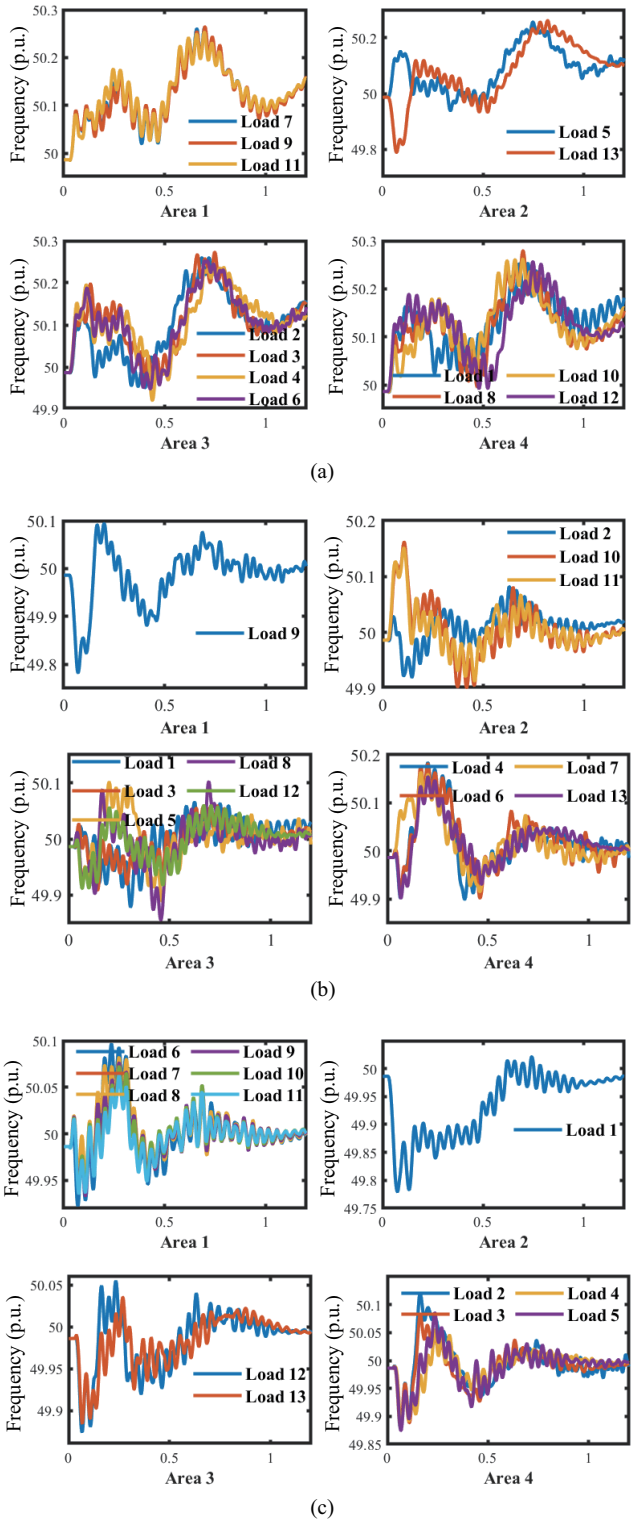

Fig. 3. The clustering results of the frequency response curves. (a) Fault 1. (b) Fault 2. (c) Fault 3.

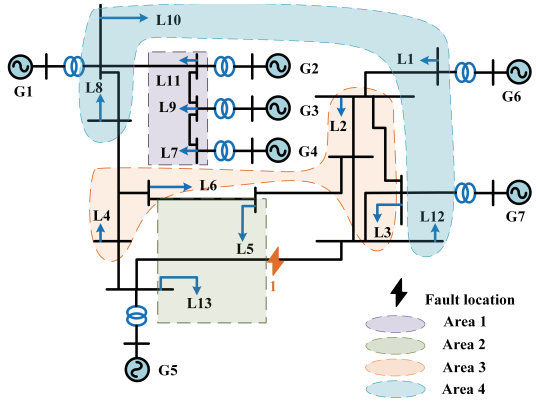

Fig. 4. System clustering results under Fault 1.

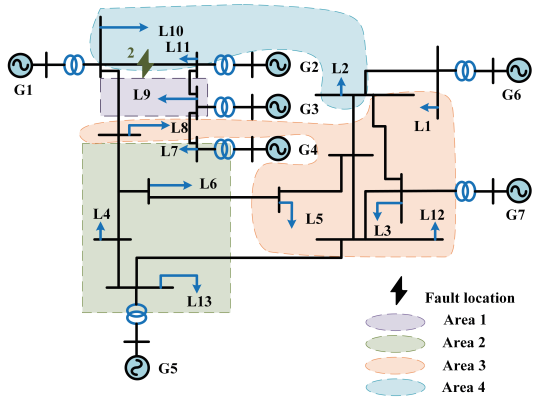

Fig. 5. System clustering results under Fault 2.

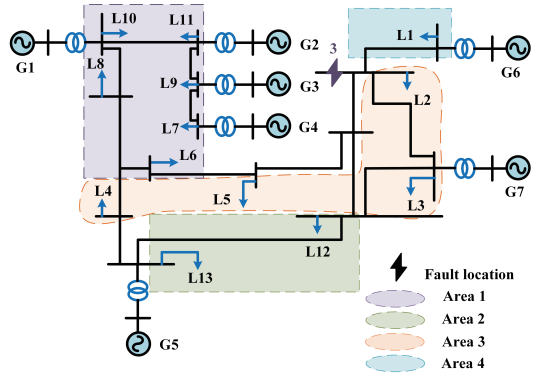

Fig. 6. System clustering results under Fault 3.

As evident from Figs. 3–6, each load exhibits varying abilities to resist faults. The frequency response data of the loads are input into the *K*-means clustering model, clustering loads with similar frequency response characteristics into the same area. However, when fault operating points change, load resistance to frequency disturbance is affected, rendering previous clustering results inapplicable to the new scenario, leading to changes in the system network clustering.

The proposed dynamic clustering method adapts to different fault scenarios, achieving corresponding clustering results, while the traditional method remains static, resulting in fixed aggregation results under varying faults. By considering the dynamic clustering of the system under multiple operating conditions, the accuracy of inertia estimation in each area is enhanced.

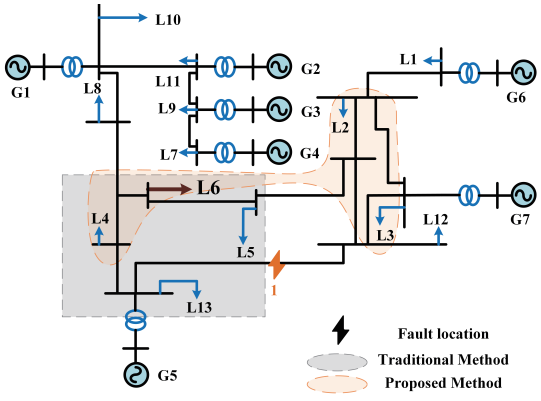

Fig. 7. Clustering of Load 6 for traditional methods and proposed methods under Fault 1.

To evaluate the proposed method's performance, its errors were compared with those of the traditional method. The accuracy of H_{area} can be demonstrated by verifying the accuracy of f_{coi} according to the mapping relationship in (12). An example involving Load 6 under Fault 1 is depicted in Fig. 7. The errors in different dimensions confirm that the proposed method outperforms the traditional method.

As depicted in Fig. 7, considering Load 6 under Fault 1 as an example, the traditional method divides loads L4, L5, L6, and L13 into a fixed area, while the proposed method employs data-driven clustering, grouping loads L2, L3, L4, and L6 into the same area. Comparing the partitioning results of the two methods, it's evident that the frequency response curves within the area in the proposed method are more similar, whereas the frequency response curves within the area in the traditional method exhibit some differences, as shown in Fig. 8.

The error curve in Fig. 8. represents the standard deviation. Standard deviation, also known as standard error, is the square root of the average of the squared deviations from the mean. It is the arithmetic square root of the variance. The standard deviation reflects the dispersion of a data set and can intuitively show the degree of deviation. The smaller the standard deviation, the less the values deviate from the mean, and vice versa.

$$\text{Error} = \sqrt{\frac{\sum_{i=1}^{N}(f_i - f_{\text{ave}})^2}{N}} \tag{13}$$

The discrepancy between the actual value and the estimated value constitutes the error, as depicted in Fig. 9. The cumulative error is illustrated in Fig. 10. MAE and RMSE are set as evaluation metrics, and the results are presented in Figs. 11 and 12.

As depicted in Fig. 11, the MAE accuracy of the proposed method is improved by 44.65%, 20.81%, and 38.44% under three different faults, respectively. Similarly, in Fig. 12, the RMSE accuracy of the proposed method is enhanced by 52.26%, 53.42%, and 47.71% under the same three faults, respectively.

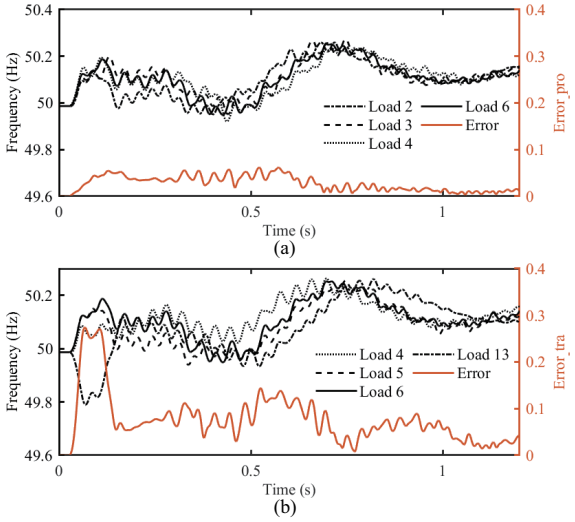

Fig. 8. The comparison of clustering results under Fault 1. (a) Proposed method. (b) Traditional method.

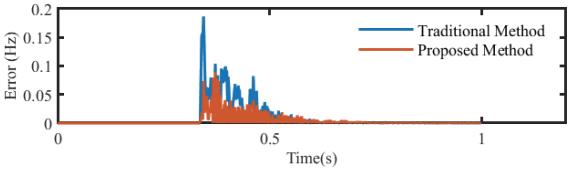

Fig. 9. Error of f_{coi} under Fault 1.

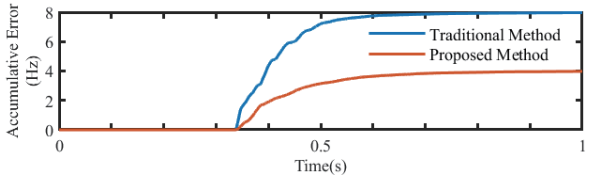

Fig. 10. Accumulative error of f_{coi} under Fault 1.

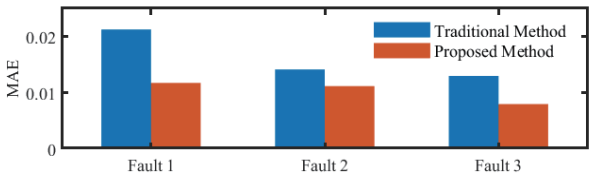

Fig. 11. MAE.

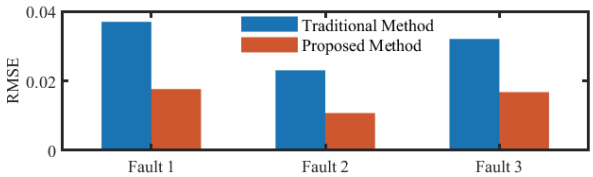

Fig. 12. RMSE.

Next, the inertia estimation model is applied to estimate the system inertia. Taking Fault 1 as an example, data from 0 to 1.5 s after the fault is selected for equivalent inertia estimation.

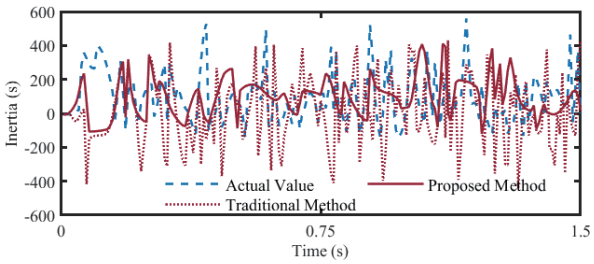

Fig. 13. Inertia estimation results under Fault 1.

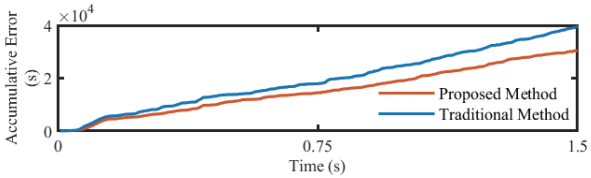

Fig. 14. Accumulative estimation error under Fault 1.

Following the frequency event, 120 sampling points are chosen from the time series data with a sampling interval of 0.0075 s. The inertia results obtained initially exhibit singular values. To address outliers, the conformal cubic interpolation (PCHIP) method is employed to fill in the outliers, and the percentile method is utilized to define the outliers, with upper and lower thresholds set to 15 and 90, respectively. Finally, the inertia estimation results are obtained, as shown in Fig. 13, while the cumulative estimation error is illustrated in Fig. 14.

Due to changes in fault transient operating points and load frequency response curves, the historical f_{coi} of the area may not be applicable to new operating conditions, leading to inaccuracies in inertia estimation using traditional methods. However, the application of the proposed method has shown promising results, indicating its effectiveness in adapting to changing system dynamics and improving the accuracy of inertia estimation.

C. Influence of Different Types of Load and Geographical Distribution Differences on System Inertia

To estimate the inertia of different types of load, a single motor and a single static load are used as examples.

As shown in Fig. 15, the inertia contributed by different types of loads has varying impacts on the system. The rotational inertia provided by motor loads is more substantial than that of static loads. To illustrate the influence of geographical distribution on system inertia, changes in the magnitude of each load distribution coefficient are considered. Specifically, load distribution scenarios are adjusted based on data from [8].

As shown in Fig. 17(b), the size of the distribution coefficient for L1 is increased by 10%, L4 is increased by 30%, L8 is increased by 45%, L5 is reduced by 10%, L9 is reduced by 25%, L11 is reduced by 55%.

As depicted in Figs. 16 and 17, variations in the geographic distribution of loads impact the system inertia distribution. Under the same disturbance, differences in load distribution

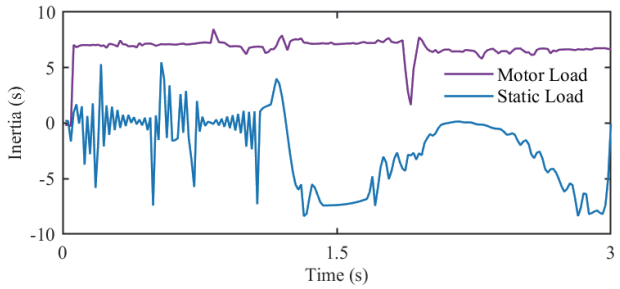

Fig. 15. Inertia estimation of motor load and static load.

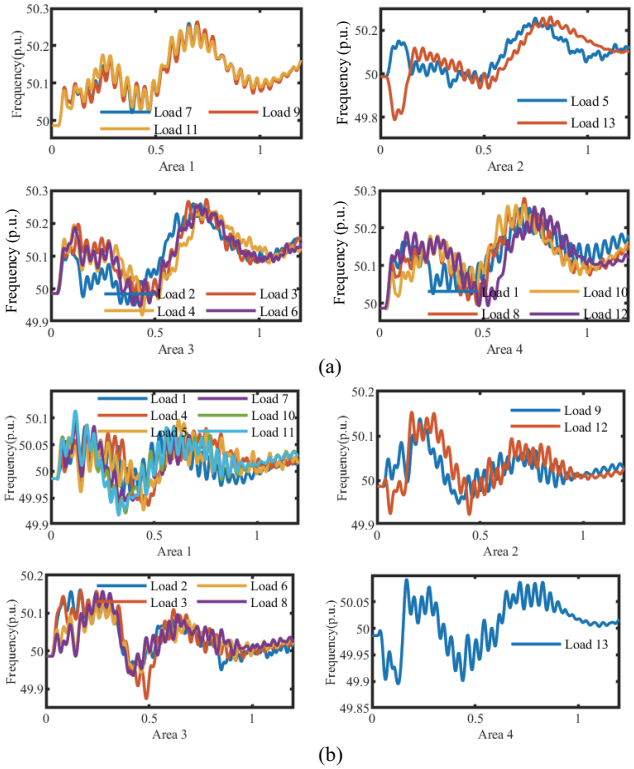

Fig. 16. The clustering results of the frequency response curves under geographical differences: (a) before and (b) after the change of load distribution coefficient.

result in distinct load frequency rate-of-change curves, which are clustered using the proposed method. Regions with similar geographic characteristics exhibit the same level of frequency, representing a uniform inertia level. This demonstrates that the inertia level within a system area shifts as the geographic distribution of loads changes.

IV. Conclusion

This paper proposes a data-driven method for estimating area equivalent inertia on the load side system, aiming to enhance the accuracy of equivalent inertia estimation. The proposed method dynamically clusters the system into equivalent areas based on the spatial distribution of inertia behavior. The study cases are conducted using the IEEE 29 buses system. Simulation results demonstrate that the proposed method achieves higher estimation accuracy than the traditional method across various transient responses.

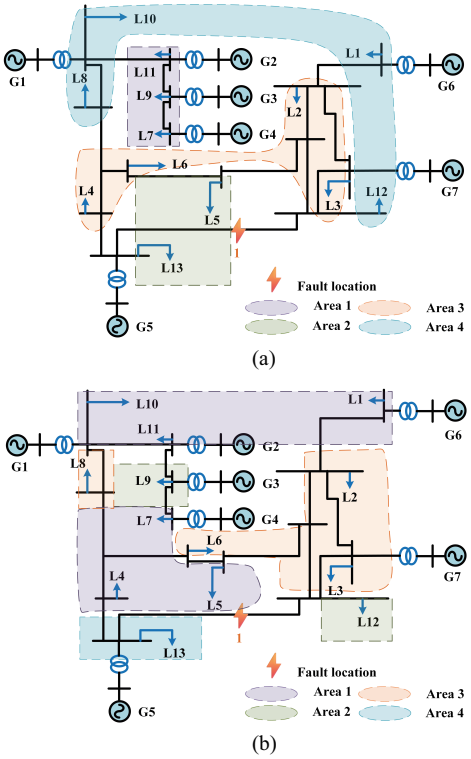

Fig. 17. System clustering results under geographical differences: (a) before and (b) after the change of load distribution coefficient.

References

[1] P. Tielens, "Operation and control of power systems with low synchronous inertia," Ph.D. dissertation, Katholieke Universiteit Leuven, Leuven, Belgium, 2017.

[2] S. Sharma, S.-H. Huang, and N. D. R. Sarma, "System inertial frequency response estimation and impact of renewable resources in ERCOT interconnection," in *2011 IEEE Power and Energy Society General Meeting*, Detroit, MI, USA, 2011, pp. 1–6.

[3] U. Tamrakar, D. Shrestha, M. Maharjan, B. P. Bhattarai, T. M. Hansen, and R. Tonkoski, "Virtual inertia: Current trends and future directions," in *Applied Sciences*, vol. 7, no. 7, Art. no. 654, Jun. 2017.

[4] E. Ørum, M. Kuivaniemi, M. Laasonen, A. I. Bruseth, E. A. Jansson, A. Danell, K. Elkington, and N. Modig, "Future system inertia," ENTSOE, Brussels, Tech. Rep., 2015.

[5] M. J. Rainey and D. T. O. Oyedokun, "Load modelling effects on power system inertia response," in *2020 IEEE PES/IAS PowerAfrica*, Nairobi, Kenya, 2020, pp. 1–5.

[6] P. Tielens and D. V. Hertem, "The relevance of inertia in power systems," in *Renewable and Sustainable Energy Reviews*, vol. 55, pp. 999–1009, Mar. 2016.

[7] H. Yin, W. Qiu, Y. Wu, S. You, J. Tan, and A. Hoke, "Field measurement and analysis of frequency and RoCoF for low-inertia power systems," in *IEEE Transactions on Industrial Electronics*, vol. 71, no. 7, pp. 7996–8006, Jul. 2024.

[8] Y. Bian, H. Wyman-Pain, F. Li, R. Bhakar, S. Mishra, and N. P. Padhy, "Demand side contributions for system inertia in the GB power system," in *IEEE Transactions on Power Systems*, vol. 33, no. 4, pp. 3521–3530, Jul. 2018.

[9] M. R. B. Tavakoli, M. Power, L. Ruttledge, and D. Flynn, "Load inertia estimation using white and grey-box estimators for power systems with high wind penetration," in *IFAC Proceedings Volumes*, vol. 45, no. 21, pp. 399–404, 2012.

[10] M. Elenkova, M. Asprou, L. Hadjidemetriou, and C. G. Panayiotou,

"Estimation of load inertia using ambient measurements from synchrophasor technology," in *2022 IEEE PES Innovative Smart Grid Technologies Conference Europe (ISGT-Europe)*, Novi Sad, Serbia, 2022, pp. 1–5.
[11] H. Thiesen and C. Jauch, "Determining the load inertia contribution from different power consumer groups," in *Energies*, vol. 13, no. 7, Art. no. 1588, Apr. 2020.
[12] R. J. Best, P. V. Brogan, and D. J. Morrow, "Power system inertia estimation using HVDC power perturbations," in *IEEE Transactions on Power Systems*, vol. 36, no. 3, pp. 1890–1899, May 2021.
[13] D. Zografos and M. Ghandhari, "Power system inertia estimation by approaching load power change after a disturbance," in *2017 IEEE Power & Energy Society General Meeting*, Chicago, IL, USA, 2017, pp. 1–5.
[14] L. Lavanya and K. S. Swarup, "Estimation of area-wise effective inertia of a power system using energy variations," in *2022 22nd National Power Systems Conference (NPSC)*, New Delhi, India, 2022, pp. 667–672.
[15] J. Shen, Y. Zhang, M. Ma, J. Yang, Q. Zhao, and S. Ke, "Data-driven equivalent inertia partition estimation of power systems," in *2022 Power System and Green Energy Conference (PSGEC)*, Shanghai, China, 2022, pp. 744–748.
[16] Y. Wang, H. Silva-Saravia, and H. Pulgar-Painemal, "Estimating inertia distribution to enhance power system dynamics," in *2017 North American Power Symposium (NAPS)*, Morgantown, WV, USA, 2017, pp. 1–6.
[17] S. You, Y. Liu, G. Kou, X. Zhang, W. Yao, and Y. Su, "Non-invasive identification of inertia distribution change in high renewable systems using distribution level PMU," in *IEEE Transactions on Power Systems*, vol. 33, no. 1, pp. 1110–1112, Jan. 2018.
[18] H. Pulgar-Painemal, Y. Wang, and H. Silva-Saravia, "On inertia distribution, inter-area oscillations and location of electronically-interfaced resources," in *IEEE Transactions on Power Systems*, vol. 33, no. 1, pp. 995–1003, Jan. 2018.
[19] Y. Xiao, X. Lin, and Y. Wen, "Multi-dimensional assessment of the inertia level of power systems with high penetration of HVDCs and renewables," in *Electric Power Construction*, vol. 41, p. 19, 2020.
[20] C. Concordia and S. Ihara, "Load representation in power system stability studies," in *IEEE Transactions on Power Apparatus and Systems*, vol. PAS-101, no. 4, pp. 969–977, 1982.
[21] P. Kundur, *Power System Stability and Control*, New York: McGraw-Hill, 1994.
[22] H. Renmu, M. Jin, and D. J. Hill, "Composite load modeling via measurement approach," in *IEEE Transactions on Power Systems*, vol. 21, no. 2, pp. 663–772, May 2006.
[23] K. Wen-Shiow, L. Chia-Jen, H. Chiang-Tsang, C. Yung-Tien, and C. Chiew-Yann, "Comparison of simulated power system dynamics applying various load models with actual recorded data," in *IEEE Transactions on Power Systems*, vol. 9, no. 1, pp. 248–254, 1994.
[24] O. H. Abdalla, M. E. Bahgat, A. M. Serag, and M. A. El-Sharkawi, "Dynamic load modelling and aggregation in power system simulation studies," in *2008 12th International Middle-East Power System Conference*, Aswan, 2008, pp. 270–276.
[25] L. Xiong, X. Liu, Y. Liu, and F. Zhuo, "Modeling and stability issues of voltage-source converter dominated power systems: A review," in *CSEE Journal of Power and Energy Systems*, vol. 8, no. 6, pp. 1530–1549, Nov. 2022.

Yunlu Li received the B.S. degree in electronic information engineering from Shenyang University of Technology in 2009, the M.S. degree in control engineering in 2011 and Ph.D. degree in power electronics and drives from Northeastern University in 2017, Shenyang, China. He worked as a post-doc researcher in Shenyang University of Technology from 2017 to 2019. He worked as a guest researcher at the Department of Energy Technology in Aalborg University, Denmark from 2018 to 2019. He is currently a Associate Professor in School of Electrical Engineering with Shenyang University of Technology, Shenyang, China. His research interests include data-driven modeling of power system, renewable energy generation technology.

Shuang Guo was born in Heihe, China, in 1999. She received the B.S. degree in automation from Shenyang University of Technology, Shenyang, China, in 2022. She is currently pursuing the M.S. degree in electrical engineering at Shenyang University of Technology, Shenyang, China. Her main research interests include microgrid modeling, distributed control, and simulation of power systems.

Guiqing Ma received the M.Sc. degree in electrical engineering from the Shenyang University of Technology, Shenyang, China, in 2023. He is currently working toward the Ph.D. degrees in electrical engineering at Shenyang University of Technology, Shenyang, China. His main research interests include system modeling, inertia estimation, and nonlinear control theory for complex dynamic system.

Zhenyu Li was born in Shenyang, China, in 1998. He received the B.S. degree in electrical engineering and automation from Suihua College, Suihua, China, in 2021. He is currently pursuing the M.S. degree in electrical engineering at Shenyang University of Technology, Shenyang, China. His main research interests include microgrid modeling, distributed control, and simulation of power systems.

Junyou Yang received the B.Eng. degree from the Jilin University of Technology, Jilin, China, the M.Sc. degree from the Shenyang University of Technology, Shenyang, China, and the Ph.D. degree from the Harbin Institute of Technology, Harbin, China. He was a Visiting Scholar with Department of Electrical Engineering and Computer Science, University of Toronto, Canada, from 1999 to 2020. He is currently the Head of the School of Electrical Engineering, Shenyang University of Technology. He is also a Distinguished Professor of Liaoning Province. His research interests include wind energy, special motor and its control.

Zhe Chen received the B.Eng. and M.Sc. degrees in electrical engineering from the Northeast China Institute of Electric Power Engineering Jilin City, China, in 1982 and 1986, and the Ph.D. degree in power and control from the University of Durham, Durham, U.K., in 1997. He is a Full Professor with the Department of Energy Technology, Aalborg University, Aalborg, Denmark. He is the Leader of Wind Power System Research program with the Department of Energy Technology, Aalborg University, and the Danish Principle Investigator for Wind Energy of Sino-Danish Centre for Education and Research. He has led many research projects and has more than 500 publications in his technical fields. His research interests include power systems, power electronics, and electric machines, wind energy and modern power systems.